# On the use and denoising of the temporal geometric mean for SAR time series

Nicolas Gasnier, Loïc Denis, Florence Tupin

# On the use and denoising of the temporal geometric mean for SAR time series

Nicolas Gasnier, *Student Member, IEEE*, Loïc Denis and Florence Tupin, *Senior Member, IEEE*

***Abstract*—The increasing availability of SAR time series creates many opportunities for remote sensing applications, but it can be challenging in terms of amount of data to process. This letter discusses the interest of the geometric mean to average SAR time series. First, the properties of the geometric mean and of the arithmetic mean are compared. Then, a speckle-reduction method specifically designed to improve images obtained with the geometric mean is presented. This method is based on an adaptation of the MuLoG framework to take into account the specific distribution of the geometric mean. Finally, applications of this denoised geometric-mean image are presented.**

***Index Terms*—ADMM, change detection, denoising, geometric mean, multi-temporal SAR series, speckle reduction, temporal mean, variational methods.**

## I. Introduction

THE availability of Synthetic Aperture RADAR (SAR) time series has substantially improved in the past few years. This has fueled many applications in domains for which the all-time acquisition capability and the repeated acquisitions of SAR sensors are essential, for example in land use monitoring or disaster detection. To study these time series, a visual summary containing the spatial structures of the scene can be very useful. By performing a temporal averaging of the images, the speckle fluctuations can be reduced and the signal-to-noise ratio of the spatial structures largely improved. The temporal arithmetic mean (temporal multi-looking) has long been used for this purpose [1]. The use of other kinds of averaging procedures such as Hölder or Lehmer means has been studied in [2]. Among these means, the geometric mean stands out for having particularly interesting properties. In particular, the geometric mean can be combined with the arithmetic mean within a likelihood ratio test to obtain a simple yet effective change detector [3]. More broadly, the multiplicative approaches demonstrated their usefulness in the processing of long SAR time series, such as in [4].

This letter focuses on the geometric mean and investigates its interest for long (more than 10 images) SAR time series analysis. The geometrical mean can be computed sequentially, leading to efficient updates when new images are available. First, we compare geometric and arithmetic means in terms of statistical properties (bias, variance, and robustness). Their behavior in various situations is studied. To further reduce the remaining speckle fluctuations in the temporal geometric mean, we derive a denoising method based on the MuLoG framework [5] that is specifically adapted to the statistical distribution of the geometric means of observed SAR intensities. The obtained geometric-mean image can be useful in various applications such as multi-temporal filtering based on a so-called "super-image" with the ratio-based framework RABASAR [6], change detection using an approach similar to MIMOSA [2], or segmentation. It also conveys useful spatial information for visual inspection.

After highlighting the interest of the geometric temporal mean with respect to the arithmetic mean in cases of reflectivity changes (temporal reflectivity fluctuations or bright outliers), the contributions of the paper are as follows:

- we introduce a way to efficiently compute numerically the probability density function of the temporal geometric mean,
- we derive an extension of MuLoG speckle reduction method [5] to account for this probability density function[1],
- we illustrate some applications of the proposed denoising method.

The remainder of the letter is organized as follows: in section II, we analyze the statistics and the properties of the geometric and the arithmetic mean. Section III presents an extension of MuLoG [5] to reduce the remaining speckle fluctuations of the geometric-mean image. Experimental results of the proposed approach are presented in section IV. Section V draws some conclusions and perspectives.

## II. Statistics of the geometric mean of SAR intensities

In this section, we study the statistics of the geometric mean of SAR images to motivate its use in the processing of SAR time series.

### A. Statistics of a SAR image

Under Goodman's hypothesis of fully developed speckle [7], the intensity follows a gamma distribution defined by the following probability density function (pdf):

$$\mathrm{p}(I|R) = \frac{L^L I^{L-1}}{\Gamma(L) R^L} \exp\left(-L\frac{I}{R}\right), \qquad (1)$$

where $I > 0$ is the observed intensity of the image, $L > 0$ is the number of looks and $R > 0$ is the reflectivity of the underlying scene.

N.Gasnier and F.Tupin are with LTCI, Télécom Paris, Institut Polytechnique de Paris, 91120 Palaiseau, France.

Loïc Denis is with Univ Lyon, UJM-Saint-Etienne, CNRS, IOGS, Laboratoire Hubert Curien UMR 5516, F-42023, St-Etienne, France.

[1]The code associated with the article is available on: https://gitlab.telecom-paris.fr/ring/geometric_mean_denoising

The distribution of the logarithm of the intensity image follows a Fisher-Tippett distribution [8] defined by the following expression, where $j = \log(I)$ and $s = \log(R)$:

$$\mathrm{p}(j|s) = \frac{L^L}{\Gamma(L)} e^{L(j-s)} \exp(-Le^{s-j}). \quad (2)$$

The expectation and the variance of $j$ are:

$$\mathbb{E}[j] = s - \log(L) + \Psi(L)\,, \quad (3)$$

$$\mathrm{Var}[j] = \Psi(1, L)\,, \quad (4)$$

where $\Psi(.)$ is the digamma function and $\Psi(.,.)$ is the polygamma function, see for example [8].

### B. Statistics of the geometric mean

The geometric mean of $T$ intensity values $I_t$ is defined by:

$$\widehat{R}_G = \sqrt[T]{\prod_{t=1}^{T} I_t} = \exp\left(\frac{1}{T}\sum_{t=1}^{T} \log I_t\right), \quad (5)$$

it corresponds to computing the exponential of an arithmetic mean of the log-transformed intensities.

If the speckle is completely decorrelated from one image to another, and if the reflectivity remains constant ($\forall t, R_t = R$), it is possible to express the probability density function of $\hat{R}_G$ using Meijer functions [9]. Using the notations introduced in [10] for Meijer functions, the pdf is given by:

$$\begin{aligned}\mathrm{p}(\widehat{R}_G|R) =& T\left(\frac{L}{R\cdot\Gamma(L)}\right)^T \widehat{R}_G^{T-1} \\ &\times \bar{G}^{T,0}_{0,T}\left(\frac{L^T\widehat{R}_G^T}{R^T}\middle|\underbrace{L-1,\ldots,L-1}_{\mathrm{T}},\overset{\cdot,\cdot}{\cdot}\right).\end{aligned} \quad (6)$$

This expression can hardly be used for numerical computations as the evaluation of Meijer functions with numerous parameters is very slow. We therefore propose an alternative to evaluate numerically the pdf in section III.

The geometric mean is affected by a bias that can be computed and compensated for:

$$\mathbb{E}[\widehat{R}_G] = \frac{R}{L}\cdot\left(\frac{\Gamma(L)}{\Gamma(\frac{L.T+1}{L})}\right)^{-T} \quad (7)$$

In the following, $\widetilde{R}_G$ is the debiased geometric mean estimator obtained by dividing $\widehat{R}_G$ by the bias, $L$ being the original number of looks of one date (here $L = 1$ for single-look images).

### C. Comparison between geometric and arithmetic means

The comparison between the geometric mean and the arithmetic mean estimators of the reflectivity performed in this section shows that while the arithmetic mean estimator is preferable when there is no change in the underlying scene, the geometric mean estimator behaves better as soon as there are significant changes of the reflectivity in at least one image of the time series. Four situations are considered: no change, fluctuations around a mean value (i.e., temporal texture), transient temporal changes, and permanent temporal changes.

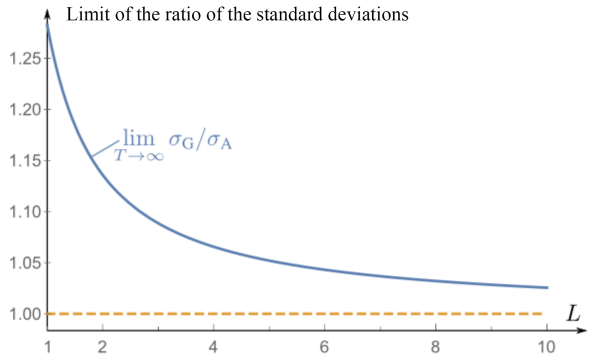


Fig. 1: Ratio $\sigma_\mathrm{G}/\sigma_\mathrm{A}$, for large values of $T$, as a function of the number of looks $L$.

*1) Situation without changes in the reflectivity, i.e., $R$ is constant over time:* When the reflectivity remains constant, the arithmetic mean estimator corresponds to the maximum likelihood estimator. The arithmetic mean of $T$ intensities, assuming a constant reflectivity and no speckle correlation, follows a gamma distribution where the number of looks $L$ is multiplied by $T$ ($L$ is thus replaced by $LT$ in equation (1)). The standard deviation $\sigma_A$ of the arithmetic mean of $T$ intensity values is:

$$\sigma_\mathrm{A} = \frac{R}{\sqrt{TL}}\,. \quad (8)$$

The standard deviation $\sigma_\mathrm{G}$ of the geometric mean estimator $\widetilde{R}_G$ can be computed through the first and the second moments of the distribution [2]:

$$\sigma_\mathrm{G} = R.L.\left(\frac{\Gamma(L)}{\Gamma(\frac{L.T+1}{L})}\right)^T \left[\frac{\Gamma(\frac{TL+2}{T})^T}{\Gamma(L)^T} - \frac{\Gamma(\frac{TL+1}{T})^{2T}}{\Gamma(L)^{2T}}\right]^{1/2} \quad (9)$$

Both estimators are consistent ($\sigma_\mathrm{A}$ and $\sigma_\mathrm{G}$ tend to zero for large values of $T$). The arithmetic mean is a more efficient estimator than the geometric mean. When $T$ is large, we obtain:

$$\lim_{T\to\infty}\frac{\sigma_\mathrm{G}}{\sigma_\mathrm{A}} = \sqrt{L\cdot\Psi(1,L)}\,. \quad (10)$$

This ratio tends to 1 when $L$ is large, as shown in figure 1. It is maximal for $L = 1$ where it is equal to $\pi/\sqrt{6} \approx 1.28$.

*2) Situation with fluctuations of the reflectivity (temporal texture):* In this paragraph we consider the case of intra-class fluctuations, inducing a temporal texture.

Although it is a well-known result that the geometric mean is more robust to strong outliers than the arithmetic mean, this paragraph shows that it is also less affected by temporal texture.

Texture models [11] have long been used to describe fluctuating reflectivities in speckle. To study the impact of these fluctuations, we ran the following experiments: a Gaussian distribution for the temporal evolution of the soil moisture is assumed. As there is a linear relationship between the log of the reflectivity and the moisture for a given soil [12], we modeled the homogeneous reflectivities with a log-normal temporal distribution with parameters $\mu_R$ and $\sigma_R$ :

$$\mathrm{p}(R|\mu_R,\sigma_R) = \frac{1}{R\sigma_R\sqrt{2\pi}}\exp\left(-\frac{(\ln R-\mu_R)^2}{2\sigma_R^2}\right). \quad (11)$$

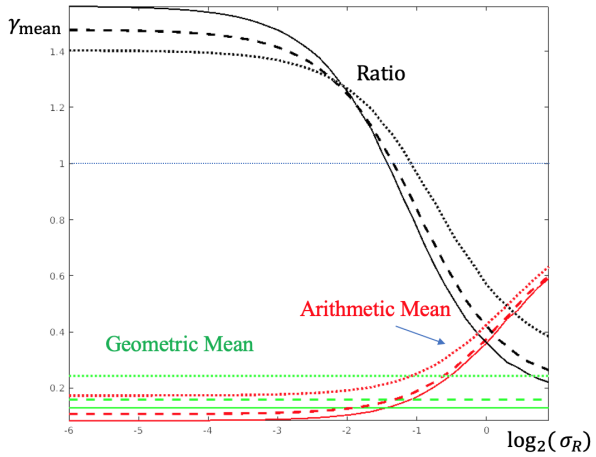


Fig. 2: Coefficient of variation of the arithmetic mean estimator $\gamma_{\mathrm{A}}$ (red) and debiased geometric mean estimator $\gamma_{\mathrm{G}}$ (green) for $\sigma_R \in [2^{-6}, 1]$ and T=12. The ratio $\gamma_{\mathrm{G}}/\gamma_{\mathrm{A}}$ is shown in black. Dotted and dashed lines correspond to simulations with temporally correlated speckle (correlations between successive images are 0.62 and 0.37, respectively).

Under this assumption, we can compare in numerical simulations the variance of the arithmetic and geometric means for various levels of variance $\sigma_R$ of the reflectivity distribution and different levels of temporal correlation. Fig. 2 shows that the coefficient of variation of the geometric mean remains constant when the temporal fluctuations $\sigma_R$ increase. In contrast, the coefficient of variation of the arithmetic mean rises with the temporal fluctuations. This behavior is confirmed for all levels of temporal correlation of the speckle considered. As soon as the temporal fluctuations are non negligible (e.g., a standard deviation $\sigma_R$ that exceeds 0.37 in the conditions of our numerical experiments: absence of temporal correlations and stack of T=12 dates), the geometric mean offers a better signal-to-noise ratio (i.e., a smaller coefficient of variation) compared to the arithmetic mean. This behavior can be easily explained: the arithmetic mean is heavily influenced by the large variance of the intensities corresponding to the largest radiometries.

The difference is also visible in real images. In figure 3, both the arithmetic mean image and the debiased geometric mean image are computed for a time series of Sentinel 1 SAR images over an area of rice fields, where the underlying reflectivity changes over time. The remaining fluctuations of the speckle noise are stronger in the arithmetic mean image (Fig.3a) than in the geometric mean image (Fig.3b).

In the case of temporal changes, the mean reflectivity obtained with the arithmetic or geometric means does not coincide with the actual reflectivities of the time series, but still provides useful geometrical information (e.g., border of fields, forests, roads, or rivers).

*3) Situation with transient temporal changes:* Bright transient changes of the reflectivity are often seen in SAR time series and can be caused by vehicles, boats, or by temporary constructions. For instance, when there is a boat visible at one date, it produces strong echoes. If we model the reflectivity

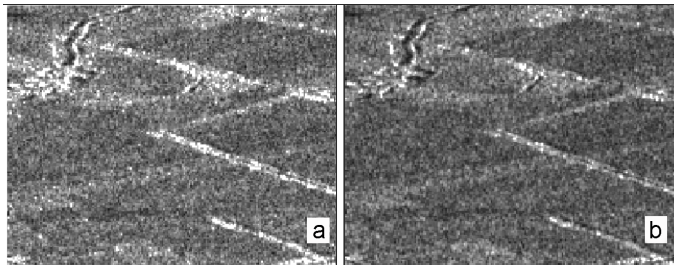


Fig. 3: Comparison of the arithmetic mean image (left) and geometric mean image (right). The fluctuations caused by the remaining noise are stronger in the arithmetic mean image.

change by a multiplication by a factor $K >> 1$ at this date, the geometric and arithmetic means are modified as follows:

- the geometric mean estimator is multiplied by $K^{\frac{1}{T}}$,
- the arithmetic mean estimator is multiplied by $1 + \frac{K-1}{T}$.

When $T > 1$, $\lim_{K\to\infty} K^{\frac{1}{T}}/(1 + \frac{K-1}{T}) = 0$, which indicates that the geometric mean is to be preferred in order to be more robust to the presence of strong scatterers at a single date: the impact of these scatterers in the mean image is much smaller. In contrast, the arithmetic mean is less sensitive to the dark counterpart of these transient changes

*4) Situation with permanent changes:* If the change is present in a large number of images, neither the arithmetic mean nor the geometric mean are good estimators of the scene. Indeed, in this situation where two classes are successively present in the time series, a single estimate cannot capture both classes. In this case, the geometric mean will bias toward the dark class while the arithmetic mean will bias toward the bright class.

In conclusion, the geometric mean has many advantages compared to the arithmetic mean, being more adapted for homogeneous classes with temporal texture and transient situations.

## III. Improving the Geometric Mean Image by Denoising

The temporal averaging reduces speckle fluctuations in the images obtained by the geometrical and arithmetic means. To further reduce the fluctuations, an additional denoising step is beneficial. In this section we extend the MuLog framework [5] to denoise images obtained with the geometric mean. MuLoG has been developed for SAR images with gamma-distributed intensities, it should thus be adapted to account for Meijer-distributed variables.

A denoised image (i.e., an image of estimated reflectivities) is obtained with MuLog by minimizing the following cost function:

$$\widehat{\boldsymbol{x}} = \underset{\boldsymbol{x}\in\mathbb{R}^n}{\arg\min}[-\log(\mathrm{p}(\boldsymbol{y}|\boldsymbol{x})) + f_{\mathrm{reg}}(\boldsymbol{x})] \qquad (12)$$

where $\boldsymbol{x}$ is the restored image, in log domain ($x_i$ is the log of the estimated reflectivity at pixel $i$), $\boldsymbol{y}$ is the log of the geometric mean image ($y_i$ corresponds to the value $\log(\widetilde{R}_G)$ at pixel $i$). The term $\log(\mathrm{p}(\boldsymbol{y}|\boldsymbol{x}))$ is the log-likelihood and the regularization function $f_{\mathrm{reg}}$ ensures that the estimated image $\widehat{\boldsymbol{x}}$

has a satisfying regularity ($f_{\text{reg}}$ can be the Total Variation (TV) or patch-based regularization like BM3D (Block Matching and 3D filtering) [5]).

The problem (12) is solved by a few iterations of the ADMM (Alternating Direction Method of Multipliers) algorithm [5], i.e., by alternating a Gaussian denoising step given in equation (13) below and the non-linear correction defined by equation (15) to account for the non-Gaussianity of speckle fluctuations in images of the geometric mean:

$$\widehat{\boldsymbol{z}} \leftarrow \underset{\boldsymbol{z}\in\mathbb{R}^n}{\arg\min} \ \frac{\beta}{2}||\boldsymbol{z} - \widehat{\boldsymbol{x}} + \widehat{\boldsymbol{d}}||^2 + f_{\text{reg}}(\boldsymbol{z})\,, \tag{13}$$

$$\widehat{\boldsymbol{d}} \leftarrow \widehat{\boldsymbol{d}} + \widehat{\boldsymbol{z}} - \widehat{\boldsymbol{x}}\,, \tag{14}$$

$$\widehat{\boldsymbol{x}} \leftarrow \underset{\boldsymbol{x}\in\mathbb{R}^n}{\arg\min} \ \frac{\beta}{2}||\widehat{\boldsymbol{z}} - \boldsymbol{x} + \widehat{\boldsymbol{d}}||^2 - \log \mathrm{p}(\boldsymbol{y}|\boldsymbol{x})\,, \tag{15}$$

where $\beta$ is a parameter that acts on the speed of convergence.

The minimization (15) can be solved with a Newton's method by using the following formula for all pixels $i$:

$$\widehat{x}_i \leftarrow \widehat{x}_i - \frac{\widehat{x}_i - \widehat{z}_i - \widehat{d}_i + \frac{D_1}{\beta}}{|1 + \frac{D_2}{\beta}|} \tag{16}$$

with $D_1$ and $D_2$ the first and second derivatives of the log-likelihood:
$D_1 = -\partial \log \mathrm{p}(y_i|x_i)/\partial x_i$ and $D_2 = -\partial^2 \log \mathrm{p}(y_i|x_i)/\partial x_i^2$.

The likelihood of the geometric mean has been defined in the intensity domain using Meijer functions in equation (6). In the log-domain, it can be defined as the iterated convolution product of Fisher-Tippett distributions. In the absence of closed-form expressions for these convolution products, it is necessary to evaluate them numerically, as well as their derivatives. We computed the convolutions as multiplications in the Fourier domain and then obtained the derivatives $D_1$ and $D_2$ by finite differences. Solutions to the problem (15) can be precomputed and stored in a table to speed-up the restoration process.

## IV. Experimental results

In order to evaluate the interest of the temporal geometric mean, we illustrate 3 different applications of the geometric mean image: to provide a high signal-to-noise ratio summary of the spatial structures from a multi-temporal stack, to detect changes, and perform multi-temporal filtering of a time series. The time series used for this experiment is composed of 20 Sentinel 1 SLC images acquired at different times but on the same orbit. In some of the images of the series, the presence of boats causes strong backscatterings.

The denoising of the geometric mean is performed by applying the BM3D denoiser [13] to update the $\widehat{\boldsymbol{z}}$ image according to equation (13), which corresponds to an implicit regularization $f_{\text{reg}}$ with edge and texture preserving properties, and the pre-tabulated solution to equation (15). To reduce the spatial correlations of speckle due to the slight over-sampling and the spectral apodization of Sentinel-1 images, a 2x2 spatial sub-sampling is applied to the time series in order to obtain images with uncorrelated speckle noise. An alternative solution is to perform a speckle decorrelation approach [14].

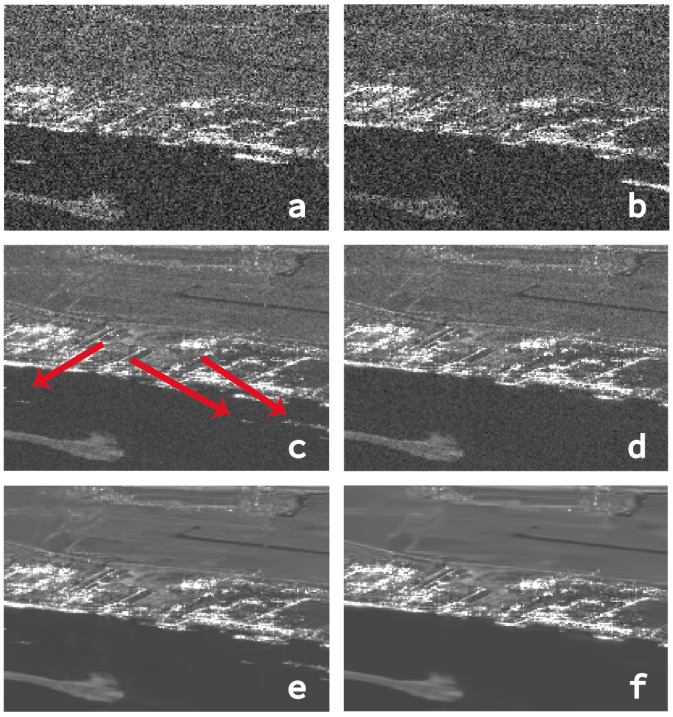


Fig. 4: Geometric vs arithmetic mean: (a) and (b) two images from the time series corresponding to dates t=11 and t=17, (c) arithmetic mean and (d) debiased geometric mean, (e) denoised arithmetic mean and (f) denoised geometric mean.

### A. Temporal summary image: comparison between arithmetic mean and geometric mean

In figure 4 both the arithmetic (c) and the geometric temporal mean (d) show an obvious improvement in term of noise level compared to the images from the time series (a and b). Nevertheless, there is still a significant level of noise in these images. As presented in section II.C, the noise level in water area (constant reflectivity) is stronger with the geometric mean than with the arithmetic mean. However, in both denoised images (e) and (f), this remaining noise has been successfully suppressed.

Concerning temporary strong scatterers, some boats that are only present at one time of the time series such as the one on the left of the 11th image of the time series (a) are clearly visible in the noisy (c) and denoised arithmetic mean (e) but not in the noisy (d) nor denoised geometric mean (f).

### B. Use of the denoised geometric mean for change detection

Comparisons of the arithmetic and geometric temporal means can be used to perform change detection [2]. The computation of denoised mean images improves detection methods based on these comparisons. For example, changes can be detected based on the ratio between the arithmetic mean and the geometric mean. Because of the residual fluctuations of speckle in the mean images, when the total number of dates is moderate, this ratio image is noisy which leads to false alarms and non-detections. Figure 5 illustrates, in the same Sentinel 1 SAR time series as in figure 2, the improvement of the ratio image brought by denoising.

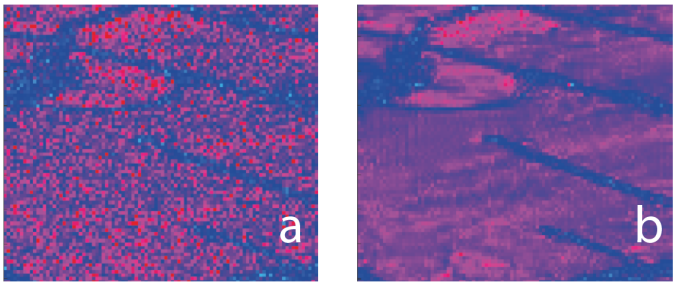


Fig. 5: Improved change detection with denoised arithmetic and geometrical means: (a) changes identified by the ratio arithmetic mean / geometric mean, (b) ratio of the denoised mean images. Stable areas are shown in blue, changing areas in red.


Fig. 6: Improved temporal filtering with a super-image obtained by denoising the geometric mean: the speckled image at the date $t = 11$ (shown in Fig.4(a)) is restored by RABASAR using a super-image obtained from (a) the arithmetic mean, or (b) the geometric mean. Note the reduction of artifacts in the circled area with the geometric mean.

### C. Use as a "super-image" for multi-temporal filtering

RABASAR [6] is a speckle reduction method for time series. It uses the arithmetic mean to produce a so-called "super-image" and to form a ratio-image where most of the spatial variability of the reflectivity is compensated for. As discussed in Section II, in the presence of an intra-class temporal texture the geometrical mean is less impacted by speckle fluctuations. It is also more robust to bright scatterers appearing only at a few dates. In these contexts, the geometrical mean leads to a better super-image and improved multi-temporal filtering results. Figure 6 shows how the restoration of an image of the time series illustrated in Fig.4 is improved when the denoised geometrical mean is used as the super-image in RABASAR: ghost structures due to transient bright scatterers (boats visible only at a few dates) are suppressed in Fig.6(b) in the circled areas. While a possible workaround to the presence of bright targets at only a few dates could consist of creating a different super-image for each image of the stack (by selecting only the dates that are sufficiently similar, as done in the original RABASAR framework [6]), this latter approach involves a significant increase of the computational load (a super-image must be re-created for each date) and does not offer improvement of the signal to noise ratio in areas with a temporal texture.

## V. Conclusion

This paper shows the benefits of using the geometric mean as a representative super-image for multi-temporal SAR data stacks and a modified approach to further reduce the speckle on this geometric-mean image. Due to the non-linear combination of speckled images in a geometrical mean, the denoising process must be carefully adapted to account for the statistical distribution of speckle in the geometrical mean image. The geometrical mean may be preferred over the arithmetic mean for several reasons: an improved robustness to the occasional presence of bright scatterers (e.g., boats) and an improved signal to noise ratio in areas with temporally fluctuating reflectivities (e.g., vegetation). Denoised geometric images can be interesting for instance to obtain a temporal summary of a multi-temporal stack of SAR images for visualization purposes. The ratio of denoised arithmetic and geometric images can also indicate changes occuring in the time series. The denoising step offers a notable improvement of the quality of the change detection map. Our method to denoise geometric mean images has also been applied to the multi-temporal filtering algorithm RABASAR and shown to effectively reduce the "ghost structures" appearing at the location of strong scatterers that were visible only at some other dates. Further studies will focus on other applications of the proposed denoising method on segmentation and multi-sensors fusion.

## Acknowledgment

The authors would like to thank the Centre National d'Études Spatiales and C-S GROUP for funding. They are grateful to the Reviewers and Associate Editor for their help in improving the paper.

## References

[1] G. Nieuwenhuis and C. Schotten, "Land cover monitoring with multi-temporal ERS-1 SAR observations in the Netherlands," in *First ERS-1 Symposium, Cannes, France*, 1992.
[2] G. Quin, B. Pinel-Puysségur, J. Nicolas, and P. Loreaux, "MIMOSA: An Automatic Change Detection Method for SAR Time Series," *IEEE TGRS*, vol. 52, no. 9, pp. 5349–5363, Sep. 2014.
[3] P. Lombardo and C. J. Oliver, "Maximum likelihood approach to the detection of changes between multitemporal SAR images," *IEE Proceedings - Radar, Sonar and Navigation*, Aug 2001.
[4] A. M. Atto, E. Trouvé, J. Nicolas, and T. T. Lê, "Wavelet operators and multiplicative observation models—application to sar image time-series analysis," *IEEE TGRS*, vol. 54, no. 11, pp. 6606–6624, 2016.
[5] C. Deledalle, L. Denis, S. Tabti, and F. Tupin, "MuLoG, or How to Apply Gaussian Denoisers to Multi-Channel SAR Speckle Reduction?" *IEEE Transactions on Image Processing*, Sep. 2017.
[6] W. Zhao, C. Deledalle, L. Denis, H. Maître, J. Nicolas, and F. Tupin, "Ratio-Based Multitemporal SAR Images Denoising: RABASAR," *IEEE TGRS*, vol. 57, no. 6, pp. 3552–3565, June 2019.
[7] J. W. Goodman, "Some fundamental properties of speckle∗," *J. Opt. Soc. Am.*, vol. 66, no. 11, pp. 1145–1150, Nov 1976.
[8] Hua Xie, L. E. Pierce, and F. T. Ulaby, "Statistical properties of logarithmically transformed speckle," *IEEE TGRS*.
[9] J. Nicolas and F. Tupin, "Statistical models for SAR amplitude data: A unified vision through Mellin transform and Meijer functions," in *2016 24th European Signal Processing Conference (EUSIPCO)*, Aug 2016.
[10] H. Bateman, *Higher transcendental functions*. McGraw-Hill, 1953.
[11] C. Oliver, "Optimum texture estimators for SAR clutter," *Journal of Physics D: Applied Physics*, vol. 26, no. 11, p. 1824, 1993.
[12] S. Bousbih, M. Zribi, Z. Lili-Chabaane, N. Baghdadi, M. El-Hajj, Q. Gao, and B. Mougenot, "Potential of Sentinel-1 Radar Data for the Assessment of Soil and Cereal Cover Parameters," in *Sensors*, 2017.
[13] K. Dabov, A. Foi, V. Katkovnik, and K. Egiazarian, "Image denoising by sparse 3-D transform-domain collaborative filtering," *IEEE Transactions on image processing*, vol. 16, no. 8, pp. 2080–2095, 2007.
[14] A. Lapini, T. Bianchi, F. Argenti, and L. Alparone, "Blind speckle decorrelation for SAR image despeckling," *IEEE TGRS*, 2014.